Monthly Notices
of the
ROYAL ASTRONOMICAL SOCIETY
MNRAS **449,** 1941–1953 (2015) doi:10.1093/mnras/stu2621

Massive stars exploding in a He-rich circumstellar medium – V. Observations of the slow-evolving SN Ibn OGLE-2012-SN-006

A. Pastorello,[1⋆] Ł. Wyrzykowski,[2,3] S. Valenti,[4,5] J. L. Prieto,[6,7] S. Kozłowski,[2] A. Udalski,[2] N. Elias-Rosa,[1] A. Morales-Garoffolo,[8] J. P. Anderson,[9] S. Benetti,[1] M. Bersten,[10,11,12] M. T. Botticella,[13] E. Cappellaro,[1] G. Fasano,[1] M. Fraser,[3] A. Gal-Yam,[14] M. Gillone,[15] M. L. Graham,[4,5] J. Greiner,[16] S. Hachinger,[1,17] D. A. Howell,[4,5] C. Inserra,[18] J. Parrent,[4,19] A. Rau,[16] S. Schulze,[7,20] S. J. Smartt,[18] K. W. Smith,[18] M. Turatto,[1] O. Yaron,[14] D. R. Young,[18] M. Kubiak,[2] M. K. Szymański,[2] G. Pietrzyński,[2,21] I. Soszyński,[2] K. Ulaczyk,[2] R. Poleski,[2,22] P. Pietrukowicz,[2] J. Skowron[2] and P. Mróz[2]

Affiliations are listed at the end of the paper

Accepted 2014 December 9. Received 2014 December 3; in original form 2014 July 29

ABSTRACT

We present optical observations of the peculiar Type Ibn supernova (SN Ibn) OGLE-2012-SN-006, discovered and monitored by the Optical Gravitational Lensing Experiment-IV survey, and spectroscopically followed by Public ESO Spectroscopic Survey of Transient Objects (PESSTO) at late phases. Stringent pre-discovery limits constrain the explosion epoch with fair precision to JD = 245 6203.8 ± 4.0. The rise time to the *I*-band light-curve maximum is about two weeks. The object reaches the peak absolute magnitude $M_I = -19.65 \pm 0.19$ on JD = 245 6218.1 ± 1.8. After maximum, the light curve declines for about 25 d with a rate of 4 mag (100 d)$^{-1}$. The symmetric *I*-band peak resembles that of canonical Type Ib/c supernovae (SNe), whereas SNe Ibn usually exhibit asymmetric and narrower early-time light curves. Since 25 d past maximum, the light curve flattens with a decline rate slower than that of the ^{56}Co–^{56}Fe decay, although at very late phases it steepens to approach that rate. However, other observables suggest that the match with the ^{56}Co decay rate is a mere coincidence, and the radioactive decay is not the main mechanism powering the light curve of OGLE-2012-SN-006. An early-time spectrum is dominated by a blue continuum, with only a marginal evidence for the presence of He I lines marking this SN type. This spectrum shows broad absorptions bluewards than 5000 Å, likely O II lines, which are similar to spectral features observed in superluminous SNe at early epochs. The object has been spectroscopically monitored by PESSTO from 90 to 180 d after peak, and these spectra show the typical features observed in a number of SN 2006jc-like events, including a blue spectral energy distribution and prominent and narrow ($v_{\rm FWHM} \approx 1900$ km s^{-1}) He I emission lines. This suggests that the ejecta are interacting with He-rich circumstellar material. The detection of broad (10^4 km s^{-1}) O I and Ca II features likely produced in the SN ejecta (including the [O I] λλ6300,6364 doublet in the latest spectra) lends support to the interpretation of OGLE-2012-SN-006 as a core-collapse event.

Key words: supernovae: general – supernovae: individual: OGLE-2012-SN-006 – supernovae: individual: SN 2006jc – supernovae: individual: SN 2010al.

1 INTRODUCTION

Supernovae of Type Ibn (SNe Ibn) are considered a rare group of stripped-envelope core-collapse (CC) events which interact with

⋆ E-mail: andrea.pastorello@oapd.inaf.it

H-depleted circumstellar material (CSM). The spectra of SNe Ibn are characterized by relatively narrow lines of He I in emission (hence the designation as 'Ibn'; Pastorello et al. 2008a), with full width at half-maximum (FWHM) velocities ranging from several hundred to a few thousand km s^{-1}. These features are thought to arise in the interactions between the SN ejecta and He-rich (and H-poor) CSM. However, weak H lines have been occasionally detected in the spectra of a few SNe Ibn, suggesting the presence of residual H in the CSM of – at least – a subsample of SNe Ibn (Pastorello et al. 2008b, 2015a; Smith et al. 2012).

The prototype of this family, SN 2006jc, has been associated with a precursor eruptive episode which occurred a couple of years before the SN explosion and reached a peak absolute magnitude $M_R \approx -14$ (Nakano et al. 2006; Yamaoka, Nakano & Itagaki 2006; Foley et al. 2007; Pastorello et al. 2007). SN 2006jc, although discovered after the maximum light, was widely studied. The brightest magnitude registered for this SN was $M_R = -18.3$ (Pastorello et al. 2007), and its optical light curve experienced a rapid post-peak decline (about 3.5 mag during the first 50 d after discovery). At later phases, the increasing decline rate of the optical light curve and the simultaneous near-infrared (NIR) excess were explained as the consequence of dust forming in a cool dense shell (e.g. Mattila et al. 2008; Smith, Foley & Filippenko 2008). Tominaga et al. (2008) and Pastorello et al. (2008b) attempted to reproduce the evolution of SN 2006jc with radioactively powered models. They both favoured models with a high kinetic energy ($E_k \sim 10^{52}$ erg), and moderate masses of ejecta ($M_{ej} \approx 4.5$–$5\ M_\odot$) and synthesized ^{56}Ni ($M_{^{56}Ni} \approx 0.2$–$0.25\ M_\odot$). None the less, radioactively powered models with even lower E_k and M_{ej} provided decent matches with observations (e.g. models A and B in Pastorello et al. 2008b, were obtained adopting the following parameters: $E_k \sim 10^{51}$ erg, $M_{ej} \leq 1\ M_\odot$ and $M_{^{56}Ni} \sim 0.25$–$0.40\ M_\odot$). On the other hand, Chugai (2009) showed that radioactive models with modest $M_{ej}/M_{^{56}Ni}$ ratio were unrealistic for a SN Ib/c explosion, and proposed that the observed parameters of SN 2006jc were best explained with strong ejecta–CSM interaction occurring already at early phases. In fact, the interaction with a circumstellar shell with mass of a few hundredths $M_\odot$ would fairly well explain the properties of SN 2006jc. It is clear, however, that for an accurate modelling good data coverage is essential along the duration of the entire SN evolution, including the very early phases, not available for SN 2006jc. The first opportunity to study an SN Ibn soon after its explosion was offered by SN 2010al, which initially showed an almost featureless spectrum with the shape of a hot blackbody (the data of this object are presented in Pastorello et al. 2015a).

The proliferation of well-organized imaging surveys, with different depths and strategies, has significantly increased the number of transients discovered and, hence, the number of Type Ibn candidates. The Optical Gravitational Lensing Experiment (OGLE; Udalski, Kubiak & Szymański 1997) is a long-term project carried out initially with the 1-m Swope telescope, and later with the 1.3-m Warsaw University Telescope, both located at the Las Campanas Observatory (LCO), Chile. The fields monitored in the course of the different seasons of the search included the two Magellanic Clouds and the Magellanic Bridge.[1] In the current fourth season (OGLE-IV; Wyrzykowski et al. 2014), which started in 2009, the survey is making use of a 32 CCD mosaic camera covering a field of 1.4 deg^2 and equipped with *V* and *I* filters. Originally conceived to study microlensing events (Paczynski 1986, 1991), a by-product of the project is the discovery of a huge number of transients and variable stars of all types, including SNe (Kozlowski et al. 2013).

The study of new types of stellar explosions is the main goal of the 'Public ESO Spectroscopic Survey of Transient Objects' (PESSTO;[2] see Smartt et al. 2013), which is a public spectroscopic survey running at the 3.58-m New Technology Telescope (NTT) of the European Southern Observatory (ESO) in La Silla (Chile). The survey is planned for four years (starting from 2012 April) and is operative 90 nights per year. The survey aims to classify a large number of transients and to monitor the most interesting objects with EFOSC2 (optical) and SOFI (NIR). Priority PESSTO targets are the most unusual SNe, SN impostors or very nearby transients, for which detailed high-quality, multiwavelength observational campaigns can be arranged.

A specific subproject has been defined within PESSTO in order to study SNe Ibn (Pastorello et al. 2008a). Two SNe Ibn discovered by the LaSilla-QUEST variability survey and followed by PESSTO (LSQ12btw and LSQ13ccw), are studied in a companion paper to this work (Pastorello et al. 2015b). A few months after LSQ12btw, a new SN Ibn candidate, OGLE-2012-SN-006, was discovered in the course of the OGLE-IV survey (Wyrzykowski, Udalski & Kozłowski 2012; Wyrzykowski et al. 2014). The object has coordinates RA = $3^h33^m34\overset{s}{.}79$ and Dec. = $-74°23'40\overset{''}{.}1$ (J2000), and lies in a faint, anonymous host galaxy (Fig. 1). According to Wyrzykowski et al. (2012), the object had a magnitude $I = 17.62$ at maximum light. OGLE-2012-SN-006 was spectroscopically classified on 2013 January 10.2 UT by Prieto & Morrell (2013) as a SN Ibn, similar to SN 2006jc. The host galaxy redshift, as estimated from the position of the narrow SN features, is $z = 0.057 \pm 0.001$. Adopting a Hubble constant value of $H_0 = 73 \pm 5\ km\ s^{-1}\ Mpc^{-1}$ ($\Omega_m = 0.27$, and $\Omega_\Lambda = 0.73$), we obtain a luminosity distance of 244.5 ± 20.0 Mpc.

Pastorello et al. (2008a), on the basis of a very small sample of objects, proposed that SNe Ibn might form a relatively homogeneous group of mildly interacting stripped-envelope SNe. However, recent discoveries suggest that SNe Ibn span a much wider range of properties than initially believed (Smith et al. 2012; Sanders et al. 2013; Gorbikov et al. 2014; Pastorello et al. 2015a,b). In this context, because of its slow-evolving light curve (see Section 2.1), OGLE-2012-SN-006 can be considered as an unprecedented addition to the SN Ibn zoo.

2 OBSERVATIONS

Our photometric and spectroscopic data have been reduced using standard procedures in the IRAF environment.[3]

Optical imaging frames were first pre-reduced (i.e. overscan, bias and flat-field corrected, and trimmed in order to remove the unexposed regions of the image). In the NIR photometry images, we also removed the contribution of the bright NIR background from the science images. Sky images were obtained by median-combining a number of dithered science frames, and were finally subtracted from each science image. In order to improve the signal

[1] A few additional fields were monitored by OGLE in the Galactic bulge and disc.

[2] http://www.pessto.org

[3] IRAF is distributed by the National Optical Astronomy Observatory, which is operated by the Association of Universities for Research in Astronomy (AURA) under cooperative agreement with the National Science Foundation.

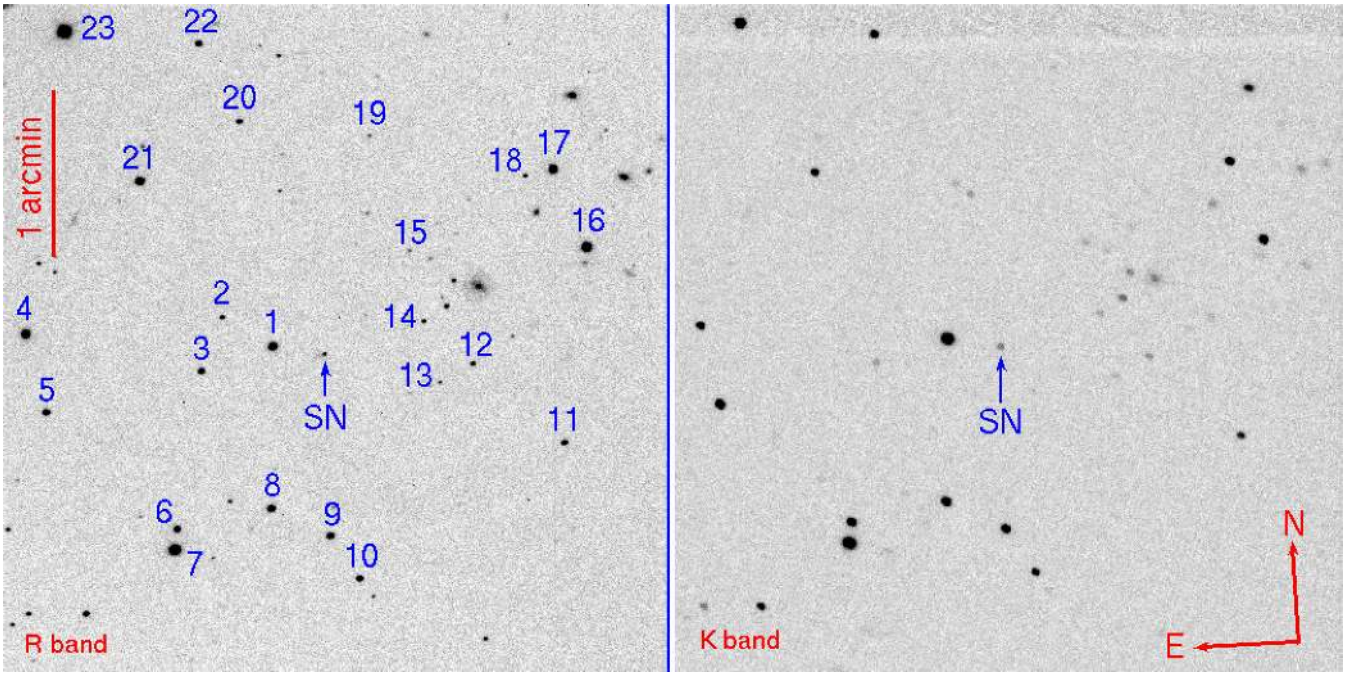

Figure 1. Left: ESO-NTT EFOSC2 *R*-band image of OGLE-2012-SN-006 obtained on 2013 January 19; the numbers mark the reference stars used to calibrate the SN magnitude. Right: ESO-NTT SOFI *Ks*-band image of OGLE-2012-SN-006 obtained on 2013 January 21.

to noise, the sky-subtracted science images were spatially registered and finally combined.

Photometric measurements in the optical and NIR bands were obtained through the PSF-fitting technique. A template PSF was built using stars in the SN field. With this PSF model along with a low-order polynomial surface, we finally performed a fit to the SN and the underlying background. OGLE-IV photometry was obtained using the difference imaging analysis, which is a template subtraction method adapted to the OGLE data and detailed in Wyrzykowski et al. 2014 (see also Woźniak 2000). The magnitudes of several stars in the SN field (see Fig. 1, left) were calibrated using observations of standard fields of the Landolt (1992) catalogue. The magnitudes obtained in photometric nights were used to estimate reliable average magnitudes for the entire local stellar sequence (23 stars), which was finally used for the calibration of the SN photometry obtained during non-photometric nights.

The NIR SN photometry was calibrated through a comparison with 14 stars of the optical sequence for which NIR magnitudes were available in the the Two Micron All Sky Survey (2MASS) catalogue (Skrutskie et al. 2006). The optical and NIR magnitudes of the SN are reported in Tables A1 and A2, while those of the local sequence stars are in Table A3. The light curves are shown in Fig. 2.

The pre-reduction process of optical spectroscopy frames followed the steps described above for photometric frames. Then, one-dimensional spectra were optimally extracted in IRAF, and wavelength calibrated using reference spectra of arc lamps. Finally, sensitivity curves obtained using spectra of spectrophotometric standards allowed us to flux-calibrate the SN spectra. Telluric absorption features were removed using normalized telluric absorption profiles derived from the spectrum of the standard star.

For the NIR spectra, two additional steps were required: first, we had to remove the intense background emission. This was achieved through the subtraction of two consecutive exposures (one from the other), since during the observation the source was dithered along

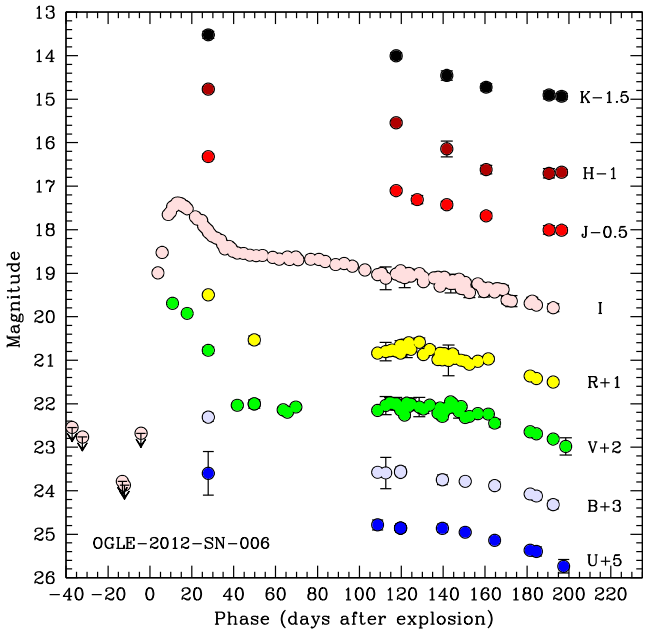

Figure 2. Optical and NIR light curves of OGLE-2012-SN-006. The light curves are shifted by the same amount indicated by the labels to the right. The phase axis is computed in days since explosion (JD = 245 6203.8 ± 4.0).

the slit direction. Secondly, we used spectra of telluric standard stars to remove the very broad (typically saturated in the NIR) atmospheric absorption bands.

Finally, the consistency of the spectroscopic flux calibration in the optical and NIR spectra was checked with available SN magnitudes and, in the case of a discrepancy, the spectral fluxes were rescaled to the photometry. The log of spectroscopic observations of OGLE-2012-SN-006 is reported in Table 1. The spectroscopic data of OGLE-2012-SN-006 are available from the ESO archive as

Table 1. Log of the spectroscopic observations of OGLE-2012-SN-006.

Date	JD−240 0000	Days since maximum	Instrumental configuration	Range (Å)	Resolution (Å)
Oct 15, 2012	562 15.81	−2.3	DuPont+B&C	3600–10 000	27
Jan 10, 2013	563 02.70	+84.6	DuPont+WFCCD	3750–9190	8
Jan 20, 2013	563 12.56	+94.5	NTT+EFOSC2+gm11+gm16	3360–10 090	14;14
Feb 20, 2013	563 43.68	+125.6	NTT+EFOSC2+gm13	3680–9300	18
Feb 22, 2013	563 45.64	+127.5	NTT+SOFI+Blue+Red	9360–25 000	24;32
Mar 18, 2013	563 69.64	+151.5	NTT+EFOSC2+gm13	3650–9300	18
Apr 19, 2013	564 02.49	+184.4	NTT+EFOSC2+gm13	3660–9280	18

PESSTO Phase 3 data products (see http://www.pessto.org) and are also available via WISeREP (Yaron & Gal-Yam 2012).[4]

2.1 Analysis of the light curves

Routine *I*-band observations of the OGLE-IV fields resulted in an excellent monitoring of the region where OGLE-2012-SN-006 exploded. OGLE-IV observations (Wyrzykowski et al. 2014) of the SN field were collected since early 2012 July, and the last non-detection was registered on 2012 September 29.26 UT. The first detection of OGLE-2012-SN-006 was on 2012 October 7.34 UT, so we can constrain the explosion epoch with a relatively small uncertainty to 2012 October 3.30 UT (JD = 245 6203.8 ± 4.0). After discovery, the object showed a relatively fast light-curve rise to *I*-band maximum, lasting ∼ 2 weeks from the adopted explosion time. Using a low-order polynomial fit to the data, we estimated the magnitude of the *I*-band light-curve maximum to be $I = 17.41 \pm 0.02$ (on 2012 October 17.6 UT, i.e. JD = 245 6218.1 ± 1.8). Adopting a distance modulus of $\mu = 36.94 \pm 0.19$ mag for the galaxy hosting OGLE-2012-SN-006 (see Section 1), assuming negligible host galaxy reddening[5] and a Galactic contribution to the total extinction of $A_I = 0.12$ mag (obtained adopting the dust map calibration of Schlafly & Finkbeiner 2011), we obtain an absolute magnitude at peak of $M_I = -19.65 \pm 0.19$. After maximum, the *I*-band light curve experienced a relatively fast decline (with a slope of $\gamma_1 \approx 4$ mag (100 d)$^{-1}$) lasting about 25 d, followed by a flattening from +25 to +70 d past maximum ($\gamma_2 \approx 0.40$ mag (100 d)$^{-1}$). Such an optical/NIR flattening, making the magnitude decline rate slower than expected for a SN powered by radioactivity of ^{56}Co, has never been observed in any SN Ibn. After that, the *I*-band light curve becomes slightly steeper ($\gamma_3 \approx 0.74$ mag (100 d)$^{-1}$), showing a slope which is closer to ^{56}Co decay (0.98 mag (100 d)$^{-1}$), but still slightly flatter than that slope. A similar decline rate in the late-time luminosity is measured in all optical bands. We note that the relatively slow late-time decline of OGLE-2012-SN-006 looks also alike to that observed in some H-rich interacting SNe, such as the SN IIn 2010jl (see below). The increased slope of the *I*-band light curve at very late phases is confirmed by a very late detection on 2013 August 1, and by deep detection limits at later epochs. This is possibly an indication of dust formation at very late phases. We note that spectroscopic indicators also support this claim (see Section 2.2).

During early phases, the evolution of OGLE-2012-SN-006 was poorly monitored in the other bands. The object was occasionally observed in the *V* band by the OGLE-IV survey, as well as in the g', r', i' Sloan bands[6] and in the NIR with the 2.2-m MPI/ESO Telescope in La Silla equipped with GROND (Greiner et al. 2008). However, after the SN classification, we realized that this was the first opportunity to monitor an SN Ibn until very late phases, since the object was showing a very slow photometric evolution. Therefore we increased the monitoring frequency of the PESSTO campaign in the optical and NIR bands using the NTT equipped with EFOSC2 and SOFI, and two 1-m LCOGT telescopes located at Cerro Tololo Inter-American Observatory. This late-time monitoring allowed us to follow in detail the late evolution of OGLE-2012-SN-006, to compute its quasi-bolometric light curve and eventually put an upper limit to the ^{56}Ni mass.

In Fig. 3 (top) the *I*-band absolute light curve of OGLE-2012-SN-006 is compared with those of SNe 2006jc, 2010al and 2010jl (the latter being a Type IIn event). For SN 2006jc we adopted $\mu = 32.01$ mag, $A_{I,\rm tot} = 0.03$ mag and JD(max) = 245 4008, for SN 2010al $\mu = 34.25$ mag, $A_{I,\rm tot} = 0.10$ mag and JD(max) = 245 5285, while for SN 2010jl $\mu = 33.45$ mag, $A_{I,\rm tot} = 0.09$ mag and JD(*I*,max) = 245 5494. The distance and the reddening adopted for OGLE-2012-SN-006 are those discussed bove. For SN 2010al the best-monitored *R*-band light curve is also shown as a comparison. OGLE-2012-SN-006 is significantly brighter than the other two SNe Ibn during its entire evolution (though fainter than SN 2010jl). We note that the early post-peak luminosity declines of SNe 2010al and 2006jc are similar, whilst OGLE-2012-SN-006 flattens quite early (at phase ∼25–30 d past maximum). However, the late-time photometric behaviour of SN 2006jc (and, possibly, SN 2010al) is mostly determined by dust formation which produces a flux deficit in the optical and an enhanced emission in the infrared domain (Mattila et al. 2008; Smith et al. 2008; Pastorello et al. 2015a). Clearly, this was not observed in OGLE-2012-SN-006. We also note that the decline rate of the *I*-band light curve of OGLE-2012-SN-006 at phases later than ∼25 d after maximum is similar to that of the SN IIn 2010jl, which showed unequivocal evidence of ejecta–CSM interaction at all evolutionary stages.

In the middle panel of Fig. 3, the $V - I$ colour curves of the above-mentioned objects are shown. We note that OGLE-2012-SN-006 becomes red very rapidly, moving from a blue colour at early stages to $V - I \approx 1.4$ mag at about 30 d after maximum. Then the $V - I$ colour turns slightly bluer in the following couple of months, and thereafter settles to about 0.8 mag. The evolution of the $V - I$ colour in SN 2006jc is quite different, since it remains almost constant (0.3–0.4 mag) until ∼50 d. Later on, it rapidly rises

[4] We note that the data presented and analysed in this paper were custom reduced, and not obtained from the First Release of PESSTO Spectral data products (SSDR1). This is because the analysis was performed before PESSTO SSDR1, and the faintness of the object required a careful treatment.

[5] From the earliest spectrum (see Section 2.2), we do not see any clear signature of the narrow interstellar Na I doublet (Na ID) at the parent galaxy redshift, suggesting little (if any) contribution of the host galaxy to the total reddening of OGLE-2012-SN-006.

[6] Sloan g', r', i' magnitudes were transformed into Johnson *B*, *V*, *R* and *I* magnitudes following the prescriptions reported in http://www.mpe.mpg.de/∼jcg/GROND/calibration.html.

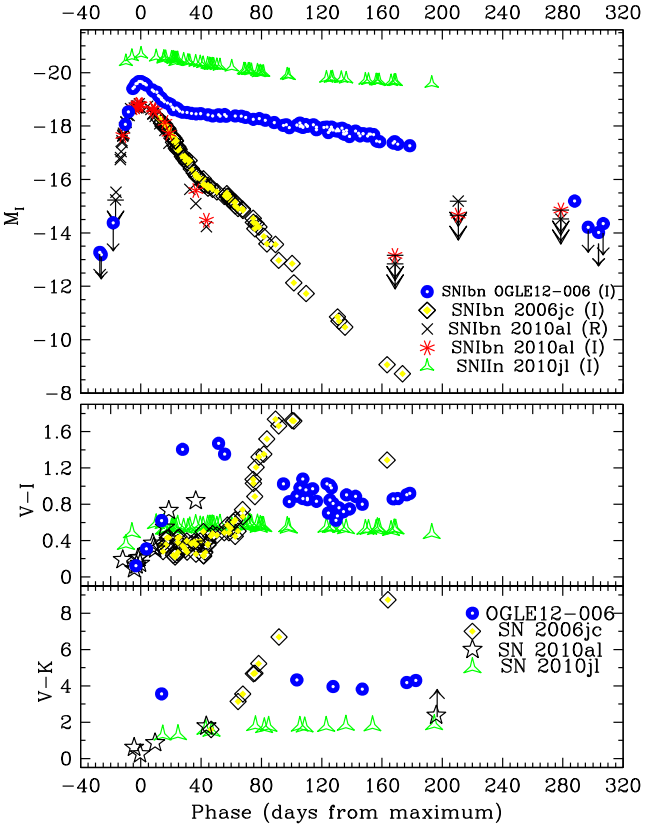

Figure 3. Comparisons of the *I*-band absolute light curves (top), $V - I$ (middle) and $V - K$ (bottom) colour curves of SNe OGLE-2012-SN-006, 2010al, 2006jc and the SN IIn 2010jl. Data of SN 2010al are from Pastorello et al. (2015a), those of SN 2006jc are from Pastorello et al. (2007), Pastorello et al. (2008b), Foley et al. (2007), Mattila et al. (2008), Di Carlo et al. (2008) and Anupama et al. (2009) and those of SN 2010jl are from Stoll et al. (2011), Zhang et al. (2012) and Fransson et al. (2014). In the top panel, together with the *I*-band light curves of the SN sample, the well-followed *R*-band light curve of SN 2010al has been included.

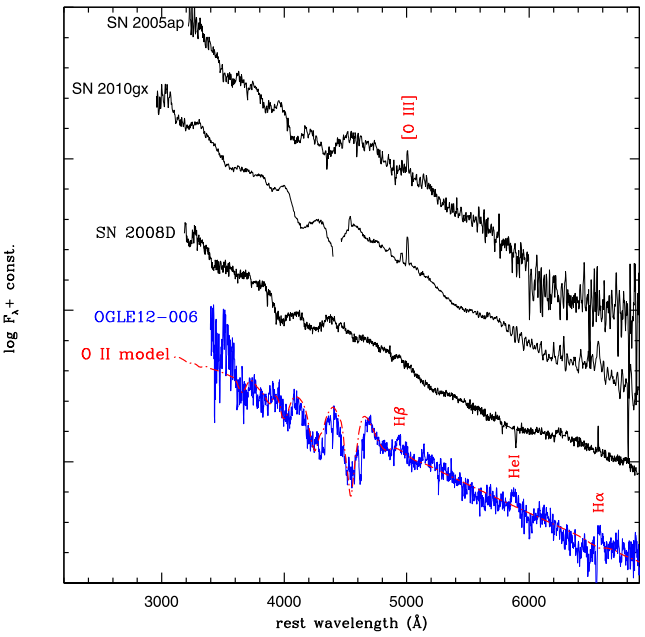

Figure 4. Comparison of our earliest spectrum of OGLE-2012-SN-006 (phase = −2.4 d from maximum) with pre-maximum spectra of other stripped-envelope SNe. Our sample includes the superluminous SNe 2005ap (Quimby et al. 2007, phase = −3.6 d from maximum) and 2010gx (Pastorello et al. 2010, time dilation corrected phase = −4.3 d from maximum), and a spectrum of the SN Ib 2008D obtained soon after the shock breakout (Modjaz et al. 2009, i.e. about 1.8 d after the X-ray burst, and −16.6 d from the *V*-band maximum). A SYNOW model, labelled as 'O II model', is overplotted to the observed spectrum of OGLE-2012-SN-006. The model was obtained adopting a continuum temperature of 11 000 K, a photospheric velocity of 7000 km s^{-1} and including a single contributing species, O II.

to $V - I \approx 1.6$ mag up to day 90, and finally declines to 1.2 mag at about 160 d. Unfortunately, for SN 2010al, the $V - I$ colour monitoring was limited only at the early phases (Pastorello et al. 2015a). However, from the available data, the evolution of the three SNe is substantially similar until day ∼20.

The bottom panel of Fig. 3 shows the $V - K$ colour evolution. Whilst the $V - K$ colour in OGLE-2012-SN-006 remains roughly constant over the entire monitored evolution ($V - K \approx 4$ mag, ranging from 3.5 mag at early phases to 4.3 mag at late phases), the $V - K$ colour of SN 2006jc shows a monotonic rise from ∼1.4 mag at 1.5 months after maximum to ∼8.8 mag at day 160. Again, the $V - K$ colour of SN 2010al is available only at early phases (from around the light-curve peak to 1.5 months after), and – in terms of time evolution – apparently mimics that of SN 2006jc. We note that colours of the SN IIn 2010jl evolve very little during the first six months of its evolution, and remain quite blue.

2.2 Spectral evolution

The object was discovered at very early stages, and the first spectrum (2012 October 15; Fig. 4), dominated by a blue, almost featureless continuum, did not allow a secure classification of the object. The temperature as obtained from a blackbody fit to the spectral continuum is 11 000 ± 1200 K. Weak lines of He I λ5876, Hα and Hβ are detected. A number of broad absorption features are visible at wavelengths shorter than 5000 Å. These absorptions somewhat resemble the O II features observed in spectra of superluminous stripped-envelope SNe (such as SNe 2005ap and 2010gx, see Fig. 4; Pastorello et al. 2010; Quimby et al. 2011) or even the putative higher ionization CNO lines detected by Modjaz et al. (2009) in the earliest spectrum of the more canonical SN Ib 2008D. In order to identify the lines in this early spectrum, we computed a model using the spectral synthesis code SYNOW (Fisher 2000). We adopt a continuum temperature of 11 000 K and a velocity at the photosphere of 7000 km s^{-1}, which is significantly lower (by a factor 2–3) than those measured in the comparison objects of Fig. 4. The contribution of O II alone is sufficient to reproduce most spectral features in the wavelengths range between 3500 and 5000 Å. We find a good match between our synthetic SYNOW spectrum and the observed one, making the identification of the spectral features as O II quite robust. However, we cannot rule out a contribution from other CNO ions, including N III, to shape the observed features in the October 15 spectrum of OGLE-2012-SN-006.

Another spectrum was obtained on 2013 January 10, and allowed Prieto & Morrell (2013) to classify the object as an SN Ibn because of the presence of strong, narrow He I lines in emission. These first two spectra of our sequence were both obtained with the 2.5-m DuPont Telescope at the LCO, the former using a B&C spectrograph, the latter with WFCCD. After the classification announcement, i.e. when the object was ∼3 months old, we started a continuous (though relaxed) PESSTO monitoring campaign using

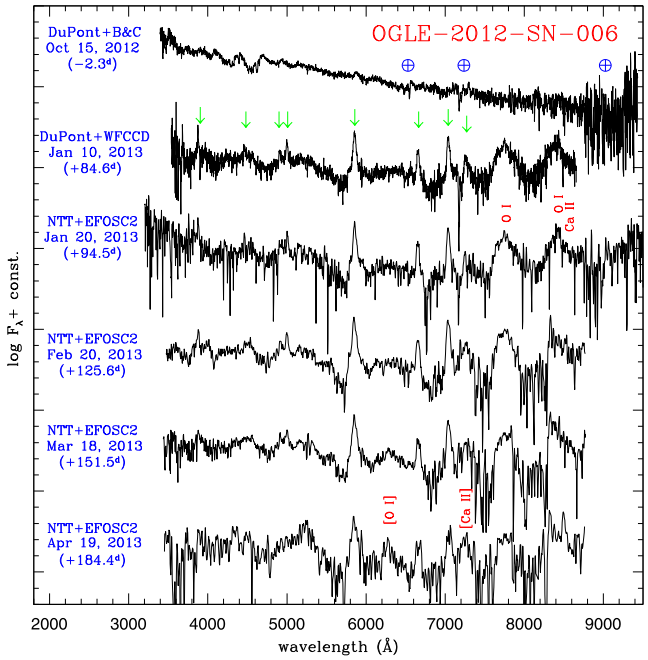

Figure 5. Sequence of optical spectra of OGLE-2012-SN-006 reported at the rest wavelength frame. The positions of the strongest He I lines are marked with green arrows. The most important SN nebular lines are also labelled. The positions of the most prominent telluric features are marked with the '⊕' symbol. The phases reported in parenthesis are days from the maximum light.

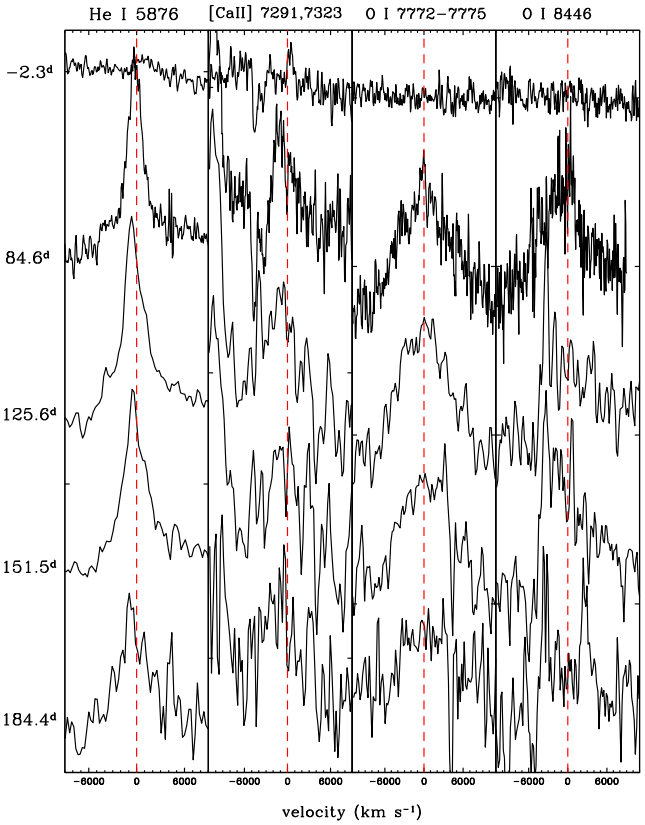

Figure 6. From the left to the right: evolution of the profiles of He I λ5876, [Ca II] λλ7291,7323, the O I λλ7772–7775 and O I λ8446. The numbers on the left indicate the phases of the spectra from the maximum light.

the NTT (with EFOSC2 and SOFI). Our complete spectral sequence is shown in Fig. 5.

The optical spectra obtained in 2013 January and February display very little evolution. They show a blue spectral energy distribution (SED), with a clear flux attenuation at wavelengths longer than about 5600 Å. The blue SED is a common property of SNe Ibn as well as other interacting events, and is possibly generated by blends of Fe emission lines (e.g. Smith et al. 2009). A very broad absorption feature, with an FWHM $\sim$ 270 Å, is detected at about 4800 Å. This is a common feature in SNe Ibn, and is probably due to Fe II lines. Much narrower He I lines are clearly detected in emission with a $v_{\rm FWHM} \approx 1300\,{\rm km\,s^{-1}}$. The strongest line at optical wavelengths is the He I λ5876 emission ($v_{\rm FWHM} \approx 2100\,{\rm km\,s^{-1}}$), possibly superposed on a less prominent, broader component ($v_{\rm FWHM} \approx 7500\,{\rm km\,s^{-1}}$).

Other prominent and narrow (but resolved) lines are He I λ6678 and He I λ7065 ($v_{\rm FWHM} \approx 1400$–$1500\,{\rm km\,s^{-1}}$). At this time, there is no evidence for the presence of a narrow Hα. The He I λ7281 emission appears to be broader than other He I lines, having $v_{\rm FWHM} \approx 2600\,{\rm km\,s^{-1}}$, though its profile may be warped by the telluric absorption band. We may also consider the possibility of a blend with nebular emission lines at about 7300 Å, such as [Ca II] λλ7291,7323 or, less likely, [O II] λλ7320,7330. Other weaker He I lines identified in the optical spectra are λ3889, λ4471, λ4922 and λ5016. At longer wavelengths, we clearly note the presence of very broad emissions identified as O I at 7772–7775 Å (possibly blended with Mg II, with $v_{\rm FWHM} \approx 10^4\,{\rm km\,s^{-1}}$), O I λ8446 and, though weaker, the NIR Ca II triplet.

The two latest spectra (obtained in 2013 March and April) show a new feature at about 6300 Å, that becomes more prominent with time. We identify it as the emerging [O I] λλ6300,6364 doublet typical of CC SNe. In addition, in the 2013 April 19 spectrum, the 7300 Å feature has now similar strength as the He I λ7065 emission. This is probably an indication of the increased contribution of the [Ca II] λλ7291,7323 (or, perhaps, [O II] λλ7320,7330) component in the blend with He I λ7281. In Fig. 6 we show the time evolution of the profiles of representative spectral lines in OGLE-2012-SN-006, in the velocity space: He I λ5876, the [Ca II] λλ7291,7323 doublet, the O I features at 7772–7775 Å and 8446 Å. In Fig. 7, late-time (three and six months past maximum) spectra of OGLE-2012-SN-006 are compared with those of the SNe Ib 1990I and 2007C at similar phases. We note than, in contrast with that observed in late SNe Ib, in OGLE-2012-SN-006 the O I λ8446 line is the most prominent feature at the red wavelengths, and largely dominates over the Ca II NIR triplet.

The He I emission lines have a slightly blueshifted peak, and the amount of blueshift increases with time, from $\sim$250 km s^{-1} in the two 2013 January spectra to about 400–500 km s^{-1} in the 2013 February–March spectra (see also Fig. 6, left-hand panel). Unfortunately, the last available spectrum (2013 April 19) has a very low signal-to-noise. However, from the position of the He I λ5876 emission, we tentatively infer a blueshift of 700 $\pm$ 150 km s^{-1}. In addition, the emission profiles show an evident asymmetry. All of this would support our claim (Section 2.1) that some dust is forming in OGLE-2012-SN-006 at late phases. We remark that in SN 2006jc the formation of dust was observed in a post-shock cool dense shell starting from $\sim$50 d after the SN explosion (Mattila et al. 2008; Smith et al. 2008). Blueshifted line emissions are frequently observed in late-time spectra of SNe IIn, and are usually considered a signature of dust formation (e.g. Gerardy et al. 2000; Fransson et al. 2005; Stritzinger et al. 2012). However, an evident blueshift of

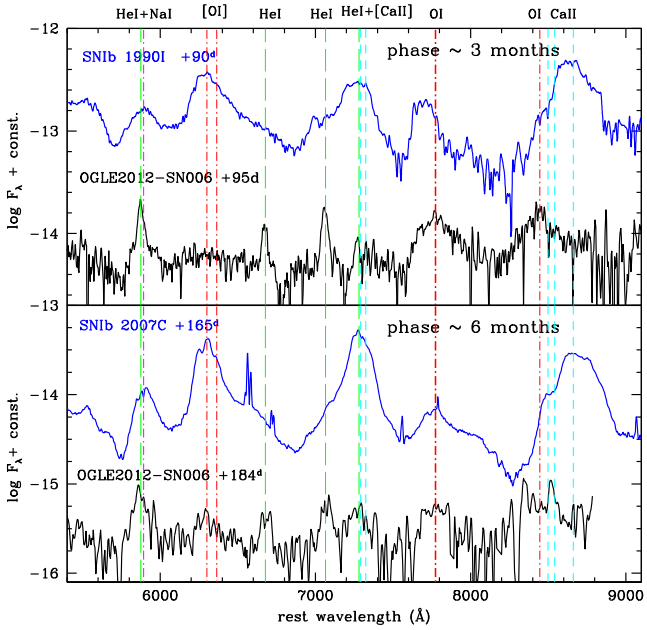

Figure 7. Top: comparison between spectra of OGLE-2012-SN-006 and the SN Ib 1990I at about three months after maximum. Bottom: a later (∼6 months) spectrum of OGLE-2012-SN-006 is compared with one of the SN Ib 2007C at a similar phase. The spectra of the comparison SNe Ib are from Taubenberger et al. (2013). The position of the most important lines is marked with vertical lines: He I (green colour), Na I (magenta), O I (red) and Ca II (cyan).

the broad Hα line component was observed in the SN IIn 2010jl (see Fransson et al. 2014, their fig. 12), and was interpreted as resulting from the bulk gas velocity, likely due to acceleration of unshocked gas by the SN radiation field.

In Fig. 8, a late-time optical + NIR spectrum of OGLE-2012-SN-006 obtained with the NTT between 2013 January 19 and 21 (at about 128 d after maximum) is compared with a VLT + XShooter spectrum of the SN Ibn 2010al (phase ∼44 d since light-curve peak) presented in Pastorello et al. (2015a). Despite the moderate signal-to-noise, the two spectra are very similar, being dominated by prominent He I lines (marked with red dot–dashed lines in the figure). In particular, the strongest He I line is the λ10830 feature. Other He I features clearly detected in the NIR spectrum of OGLE-2012-SN-006 are the λ17002 and λ20581 lines, and a blend at around 18690 Å. We also notice the overall similarity of the two spectra in the optical domain, both showing the prominent blend formed by O I λ8446 with the NIR Ca II triplet, while the O I λ7774 feature is much stronger in the spectrum of OGLE-2012-SN-006 (although it is clearly detected also in SN 2010al).

3 DISCUSSION AND SUMMARY

OGLE-2012-SN-006 is an interesting object owing to its unprecedented properties in the context of the SN Ibn family. An early-time spectrum shows a blue continuum and broad absorptions probably due to CNO elements (mostly O II), that are not frequently observed in classical CC SN spectra. These spectral features are similar to those observed in superluminous stripped-envelope

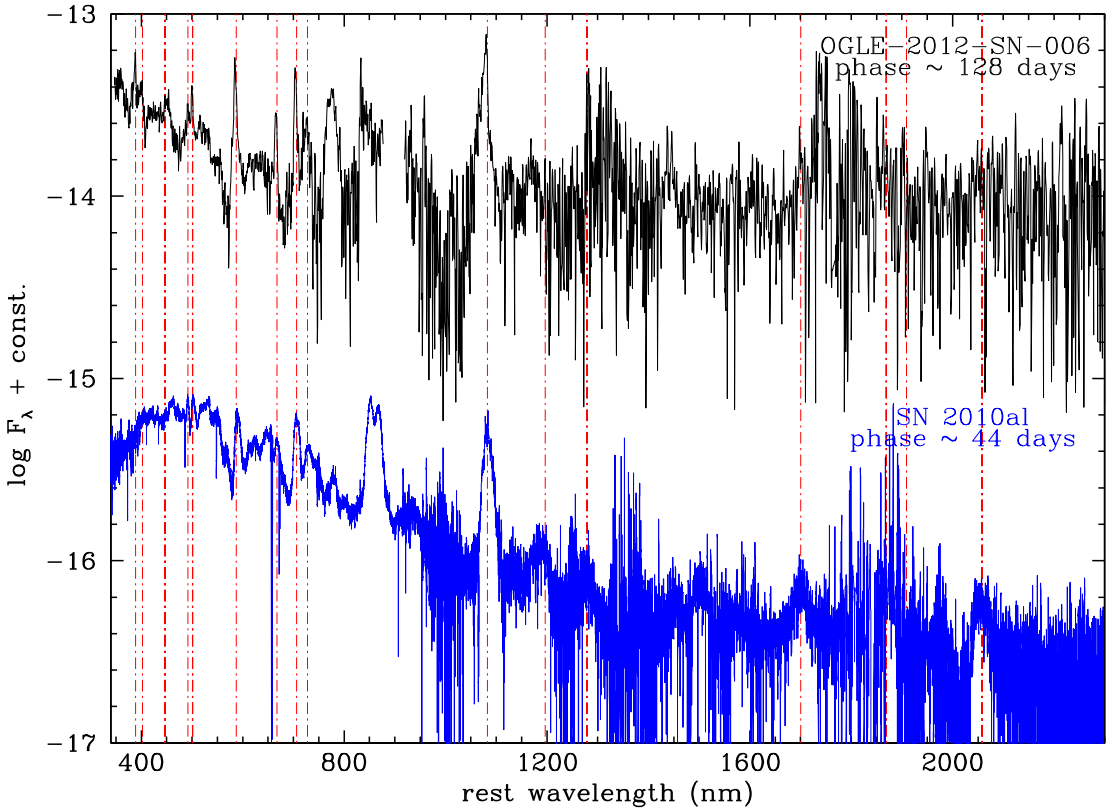

Figure 8. Optical + NIR spectrum of OGLE-2012-SN-006 (∼128 d after maximum) compared with an XShooter spectrum of SN 2010al (Pastorello et al. 2015b) obtained when the SN was about 44 d past maximum (i.e. two months after the explosion). The red dot–dashed lines mark the position of the strongest He I features. The two spectra have been redshift-corrected. Both objects show rather prominent features of O I λ7774 (much stronger in OGLE-2012-SN-006), and O I λ8446 plus the Ca II NIR triplet.

transients (Quimby et al. 2011). The post-peak optical and NIR light curves show a fast decline until about one month after the explosion. Then the light curves level off to a very slow decline rate. In coincidence with the late curve flattening, the spectra show the relatively narrow He I in emission typical of the SN Ibn family, which are interpreted in terms of interaction with He-rich CSM. The late light-curve tail has initially a flat slope, although later (starting from about four months after the explosion) it shows a decline rate similar to that expected when the powering mechanism is the radioactive decay of ^{56}Co into ^{56}Fe. The optical light curves of the prototype SN 2006jc showed a much faster decline in the optical bands and an increasing luminosity in the IR domain. This was interpreted as a signature of dust formation (Di Carlo et al. 2008; Mattila et al. 2008; Nozawa et al. 2008; Smith et al. 2008; Sakon et al. 2009) in a post-shock cool and dense circumstellar shell. However, there is evidence of an increasing slope in the late-time *I*-band light curve in OGLE-2012-SN-006, which may be attributed to dust formation also in this case.

An important issue that we have not yet discussed is the physical mechanisms that could power the bright peak luminosity and the unprecedented photometric evolution of the Type Ibn OGLE-2012-SN-006. For this goal, we have calculated a (quasi)-bolometric light curve for OGLE-2012-SN-006 by integrating the flux contribution in individual optical and NIR passbands. In practice, for each epoch with *I*-band observations available and for each band, we derived the flux at the effective wavelength. When photometric points in individual bands were not available at a given epoch, their contribution was estimated through an interpolation of photometry in adjacent epochs. Unfortunately, early-time photometry was available for OGLE-2012-SN-006 only in the *I* and (to a lesser extent) in the *V* band. The flux contribution of the missing bands at early phases, in particular during the rising branch to the peak and the period around maximum, has been obtained under the rough assumption that the early colour evolution of OGLE-2012-SN-006 was similar to that of the SN Ibn 2010al (Pastorello et al. 2015a). Although the colour evolutions of SNe 2010al and OGLE-2012-SN-006 are very different, there is a good match in the early-time optical colours (up to ∼15 d past maximum; see Fig. 3, middle panel). The fluxes, corrected for the adopted extinction, provide the SED at the given phase, which are then integrated through the trapezoidal rule. The observed flux is finally converted to luminosity adopting the distance and interstellar reddening values mentioned above. We did not account for flux contribution beyond the observed *U* and NIR bands, and therefore this has been more properly quoted as a 'quasi-bolometric' light curve. We should emphasize that the luminosity contribution of the ultraviolet (UV) domain, especially at early phases, may be significant (see e.g. Pastorello et al. 2015a). The resulting quasi-bolometric light curve is shown in Fig. 9.

Although we have limited information on the spectroscopic and photometric evolution of OGLE-2012-SN-006, we attempt to constrain SN parameters using the quasi-bolometric light curve computed before, with the initial assumption that the SN luminosity peak is mostly powered by the radioactive decays. To this aim, we fit the SN data using a toy light-curve model elaborated by Valenti et al. (2008),[7] which has been shown to successfully reproduce the early-phase bolometric light curves of various stripped-envelope SNe. The model of Valenti et al. (2008) is based on simple analytical approximations (Arnett 1982; Cappellaro et al. 1997; Clocchiatti & Wheeler 1997), and on a division of the light curve into two periods. In the first period, the supernova is optically thick (photospheric phase); later on, it gets optically thin (nebular phase). The model assumes that – at least in the early phase (<50 d) – the CSM–ejecta interaction does not provide a major contribution to the observed bolometric luminosity. By assessing the model consistency, we will make an effort to test this assumption, although it may appear natural since the early light curve of OGLE-2012-SN-006 resembles those of radioactively-powered SNe Ia and/or SNe Ib/c , and our earliest spectrum shows no narrow emission lines from interaction. The comparison between the bolometric light curve of OGLE-2012-SN-006 and our best light-curve model of a radioactively powered stripped-envelope SN is shown in Fig. 9 (the parameters used for the model are illustrated in the figure caption). If the SN radiation is powered by radioactive decays, this would imply a relatively high kinetic energy and extremely small ejecta mass, a large fraction of which would be ^{56}Ni. The inferred M(^{56}Ni)/$M_{\rm ej}$ ratio (∼0.5) is similar to those estimated in some luminous SNe Ia (e.g. Taubenberger et al. 2013), but are not comfortably accommodated in the context of a CC explosion scenario. We also note the late-time spectra are dominated by He and α-elements, and not by iron-peak elements. All of this clearly argues against the initial assumptions adopted for the model, and suggests that the ^{56}Ni to ^{56}Co to ^{56}Fe decay chain is not the primary process which powers the light curve of OGLE-2012-SN-006. As a consequence, ejecta–CSM interaction provides a more plausible explanation.

We note, however, that a degenerate progenitor system scenario had been previously proposed by Sanders et al. (2013) for another

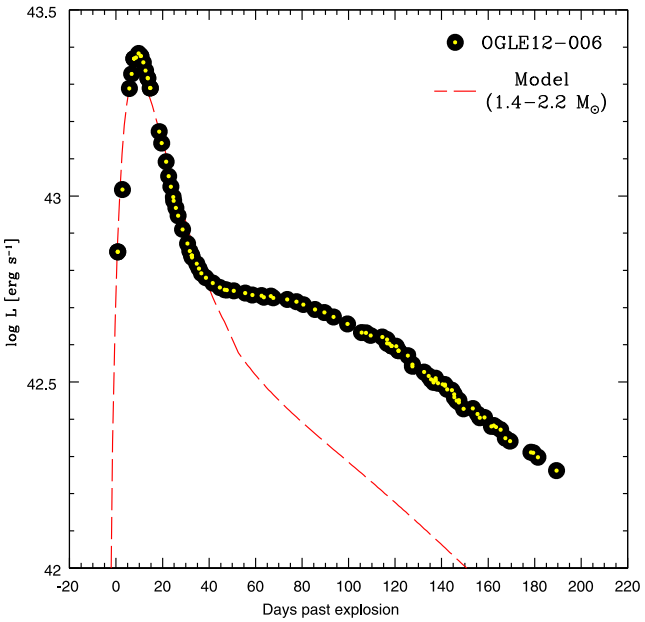

Figure 9. Comparison between the pseudo-bolometric light curve of OGLE-2012-SN-006 and a radioactively-powered light-curve model. As we have limited information on the ejecta velocity at the time of the light-curve peak, we assume that the photospheric velocity at maximum is $v = 15\,000 \pm 1000$ km s^{-1}. We adopt an optical opacity of $\chi = 0.1$ cm^2 g^{-1}. A model which provides a decent match with the observed quasi-bolometric light curve of OGLE-2012-SN-006 at early phases, is obtained adopting the following parameters: M(^{56}Ni) = 0.8–1.1 M$_\odot$, $M_{\rm ej}$ = 1.4–2.2 M$_\odot$, $E_{\rm k}$ = 1.3–7.5 × 10^{51} erg. Clearly, a poor match is obtained with the late-time light curve of OGLE-2012-SN-006.

[7] This model is obtained using the code of Valenti et al. (2008), which is based on Arnett (1982), but accounting for the typo correction reported in Arnett (1996) – see Wheeler, Johnson & Clocchiatti (2014).

SN Ibn, PS1-12sk. The unusual location of that object in the outskirts of an elliptical galaxy, suggested a progenitor scenario which could have been different from the canonical CC of a massive, stripped-envelope star normally assumed for SNe Ibn, including the possibility of a white dwarf explosion in a He-rich environment (Sanders et al. 2013). However, to our knowledge, this still remains a unique case in the SN Ibn zoo, since all other objects exploded in spiral galaxies (Pastorello et al. 2015b). In addition, as admitted by Sanders et al. (2013), some residual star formation at the SN location and/or the association with a nearby, low-luminosity dwarf galaxy cannot be ruled out, and – consequently – the progenitor may still be a massive star.

The fact that SNe Ibn explode preferentially in young stellar population environments, the pre-SN eruption detected in SN 2006jc and – even more – the detection of the [O I] λλ6300,6364 doublet in the late spectra of OGLE-2012-SN-006, are robust arguments to support a CC scenario for SNe Ibn. As mentioned before, the high M(^{56}Ni)/$M_{\rm ej}$ ratio estimated for OGLE-2012-SN-006 from the model described above, can be explained with incorrect initial assumptions on the source powering the early light curve of this object. In other words, the high luminosity at peak may have not been completely due to radioactive decay. In the view of the presence of a dense He shell, we argue that other processes may give a significant contribution to the total SN luminosity around maximum light. As a consequence, the assumptions from using the toy model are violated, and the progenitor and explosion parameters are likely to be significantly different from those derived in the simple model fits. Almost certainly the explosion of OGLE-2012-SN-006 produced a smaller amount of ^{56}Ni and a larger ejecta mass.

In this context, there is an appealing qualitative similarity between the quasi-bolometric light curve of OGLE-2012-SN-006 and the light-curve models discussed in Falk & Arnett (1977). In particular, there is a surprising match with the light-curve models obtained considering a stellar ejected envelope plus an overlying circumstellar shell (Models B of Falk & Arnett 1977, see e.g. their fig. 10). According to these models, the luminous peak would be the result of radiative heating and diffusion of radiation ahead of the shock front in a low-density circumstellar shell. Modern simulations of this class of interaction-powered SNe have been presented in detail, for example, by Moriya et al. (2011). According to Moriya & Tominaga (2012), the absence of prominent narrow lines, as in the case of the early spectrum of OGLE-2012-SN-006, would not be an indication of lack of interaction. Instead, it could be related with a non-steady mass-loss of the progenitor prior to the explosion. Although this scenario was used to explain the early behaviour of H-rich SNe, it might be extended to Type I events, such as OGLE-2012-SN-006. However, while in the case of the models of Falk & Arnett (1977) or Moriya et al. (2011) the H envelope recombination sets the post-peak luminosity evolution, in SNe Ibn the ejecta–CSM interaction is probably the preponderant source of energy powering the light curve until late phases.

The precursors of SNe Ibn have been proposed to be H-depleted, He-rich (i.e. 'WN' type; Foley et al. 2007) Wolf–Rayet (WR) stars or more He-poor (of 'WC-O' type; Pastorello et al. 2007; Tominaga et al. 2008) WR stars. In addition, a few rare and moderately H-rich Ibn events, such as SNe 2005la and 2011hw, have been proposed to be produced by stars that were transiting from luminous blue variable to WR stages (e.g. WN-type; Smith et al. 2012; Pastorello et al. 2015a). In this context, the spectra of OGLE-2012-SN-006 show very little evidence for the presence of H lines (and only in the first spectrum), thus suggesting that the precursor was an almost totally H-depleted WR star that suffered major mass-loss processes before exploding as a CC SN.

So far, we have collected incomplete information from an increasing number of SNe Ibn. In order to increase our knowledge on this SN family, we need to promptly detect a young SN Ibn just after explosion, and follow it until the nebular phase. With OGLE-2012-SN-006, we partly reached that aim, since we collected valuable information on the evolution of a SN Ibn until very late phases. However, because of the slow reaction of the astronomical community and the unusual properties of the early-time spectrum, it was not promptly classified. As a consequence, we missed the opportunity to better sample the impressive spectral metamorphosis at early times that can be only inferred from the available data. In addition, we did not target OGLE-2012-SN-006 in the UV domain, which is crucial to properly estimate the UV contribution to the total luminosity during the first few days after the explosion. An efficient cooperation and exchange of information within the astronomical community is essential to achieve these goals, and we aim to do this as soon as a new suitable young SN Ibn will become available.

ACKNOWLEDGEMENTS

We would like to thank the anonymous referee for providing us with constructive comments and suggestions.

AP, EC, SB and MT are partially supported by the PRIN-INAF 2011 with the project 'Transient Universe: from ESO Large to PESSTO'. NER acknowledges the support from the European Union Seventh Framework Programme (FP7/2007-2013) under grant agreement no. 267251 Astronomy Fellowships in Italy (AstroFIt). AMG acknowledges financial support by the MICINN grant AYA2011-24704/ESP, by the ESF EUROCORES Program EuroGENESIS (MINECO grants EUI2009-04170), SGR grants of the Generalitat de Catalunya and by the EU-FEDER funds. This work was partially supported by the Polish Ministry of Science and Higher Education through the program 'Ideas Plus award no. IdP2012 000162. SS acknowledges support from CONICYT-Chile FONDECYT 3140534, Basal-CATA PFB-06/2007, and Project IC120009 'Millennium Institute of Astrophysics (MAS)' of Iniciativa Científica Milenio del Ministerio de Economía, Fomento y Turismo.

Research leading to these results has received funding from the European Research Council under the European Union's Seventh Framework Programme (FP7/2007-2013)/ERC Grant agreement no. [291222] (PI: SJS) and EU/FP7-ERC grant no. [307260] (PI: AG-Y). AG-Y is also supported by The Quantum Universe I-Core programme by the Israeli Committee for planning and funding and the ISF, a GIF grant, and the Kimmel award. The OGLE project has received funding from the European Research Council under the European Community's Seventh Framework Programme (FP7/2007-2013)/ERC grant agreement no. 246678 to AU. This work is partially supported by the Polish Ministry of Science and Higher Education program "Ideas Plus" no. IdP2012 000162, and is also partly supported by the European Union FP7 programme through ERC grant number 320360.

This work is partially based on observations obtained under the ESO-NTT Large Program 188.D-3003 (PESSTO). This work makes use of observations from the LCOGT network, the 1.3-m Warsaw University Telescope and the 2.5-m du Pont Telescope at the LCO, the 2.2-m MPI/ESO Telescope and the 3.58-m ESO NTT at ESO-La Silla.

We thank Jonathan Elliott (MPE Garching) for executing the GROND observation. AP thanks M. L. Pumo for useful discussions. Part of the funding for GROND (both hardware as well as personnel) was generously granted from the Leibniz-Prize to Professor G. Hasinger (DFG grant HA 1850/28-1).

This publication makes use of data products from the 2MASS, which is a joint project of the University of Massachusetts and the Infrared Processing and Analysis Center/California Institute of Technology, funded by the National Aeronautics and Space Administration (NASA) and the National Science Foundation. This research has made use of the NASA/IPAC Extragalactic Database (NED) which is operated by the Jet Propulsion Laboratory, California Institute of Technology, under contract with the NASA. We acknowledge the usage of the HyperLeda data base (http://leda.univ-lyon1.fr).

REFERENCES

Anupama G. C., Sahu D. K., Gurugubelli U. K., Prabhu T. P., Tominaga N., Tanaka M., Nomoto K., 2009, MNRAS, 392, 894
Arnett W. D., 1982, ApJ, 253, 785
Arnett W. D., 1996, Supernovae and Nucleosynthesis: An Investigation of the History of Matter, from the Big Bang to the Present. Princeton Univ. Press, Princeton, NJ
Cappellaro E., Mazzali P. A., Benetti S., Danziger I. J., Turatto M., della Valle M., Patat F., 1997, A&A, 328, 203
Chugai N. N., 2009, MNRAS, 400, 866
Clocchiatti A., Wheeler J. C., 1997, ApJ, 491, 375
Di Carlo E. et al., 2008, ApJ, 684, 471
Falk S. W., Arnett W. D., 1977, ApJS, 33, 151
Fisher A., 2000, PhD Thesis, Univ. Oklahoma
Foley R. J., Smith N., Ganeshalingam M., Li W., Chornock R., Filippenko A. V., 2007, ApJ, 657, L105
Fransson C. et al., 2005, ApJ, 622, 991
Fransson C. et al., 2014, ApJ, 797, 118
Gerardy C. L., Fesen R. A., Höflich P., Wheeler J. C., 2000, AJ, 119, 2968
Gorbikov E. et al., 2014, MNRAS, 443, 671
Greiner J. et al., 2008, PASP, 120, 405
Kozłowski S. et al., 2013, Acta Astron., 63, 1
Landolt A. U., 1992, AJ, 104, 340
Mattila S. et al., 2008, MNRAS, 389, 141
Modjaz M. et al., 2009, ApJ, 702, 226
Moriya T. J., Tominaga N., 2012, ApJ, 747, 118
Moriya T., Tominaga N., Blinnikov S. I., Baklanov P. V., Sorokina E. I., 2011, MNRAS, 415, 199
Nakano S., Itagaki K., Puckett T., Gorelli R., 2006, Cent. Bur. Electron. Telegrams, 666, 1
Nozawa T. et al., 2008, ApJ, 684, 1343
Paczynski B., 1986, ApJ, 304, 1
Paczynski B., 1991, ApJ, 371, L63
Pastorello A. et al., 2007, Nature, 447, 829
Pastorello A. et al., 2008a, MNRAS, 389, 113
Pastorello A. et al., 2008b, MNRAS, 389, 131
Pastorello A. et al., 2010, ApJ, 724, L16
Pastorello A. et al., 2015a, preprint (arXiv:1502.04946)
Pastorello A. et al., 2015b, preprint (arXiv:1502.04949)
Prieto J. L., Morrell N., 2013, Astron. Telegram, 4734, 1
Quimby R. M., Aldering G., Wheeler J. C., Höflich P., Akerlof C. W., Rykoff E. S., 2007, ApJ, 668, 99
Quimby R. M. et al., 2011, Nature, 474, 487
Sakon I. et al., 2009, ApJ, 692, 546
Sanders N. E. et al., 2013, ApJ, 769, 39
Schlafly E. F., Finkbeiner D. P., 2011, ApJ, 737, 103
Skrutskie M. F. et al., 2006, AJ, 131, 1163
Smartt S. J. et al., 2013, The Messenger, 154, 50
Smith N., Foley R. J., Filippenko A. V., 2008, ApJ, 680, 568
Smith N. et al., 2009, ApJ, 695, 1334
Smith N., Mauerhan J. C., Silverman J. M., Ganeshalingam M., Filippenko A. V., Cenko S. B., Clubb K. I., Kandrashoff M. T., 2012, MNRAS, 426, 1905
Stoll R., Prieto J. L., Stanek K. Z., Pogge R. W., Szczygieł D. M., Pojmański G., Antognini J., Yan H., 2011, ApJ, 730, 34
Stritzinger M. et al., 2012, ApJ, 756, 173
Taubenberger S. et al., 2013, MNRAS, 432, 3117
Tominaga N. et al., 2008, ApJ, 687, 1208
Udalski A., Kubiak M., Szymański M., 1997, Acta Astron., 47, 319
Valenti S. et al., 2008, MNRAS, 383, 1485
Wheeler J. C., Johnson V., Clocchiatti A., 2014, MNRAS, preprint (arXiv:1411.5975)
Woźniak P. R., 2000, Acta Astron., 50, 421
Wyrzykowski Ł., Udalski A., Kozłowski S., 2012, Astron. Telegram, 4495, 1
Wyrzykowski Ł. et al., 2014, Acta Astron., 64, 197
Yamaoka H., Nakano S., Itagaki K., 2006, Cent. Bur. Electron. Telegrams, 666, 2
Yaron O., Gal-Yam A., 2012, PASP, 124, 668
Zhang T. et al., 2012, AJ, 144, 131

APPENDIX A: PHOTOMETRY OF OGLE-2012-SN-006

Table A1. Optical photometry of OGLE-2012-SN-006.

Date (dd-mm-yy)	JD (+240 0000)	*U*	*B*	*V*	*R*	*I*	Instrument
03-07-12	561 11.92	–	–	–	–	> 21.16	1
16-07-12	561 24.93	–	–	–	–	> 22.29	1
11-08-12	561 50.88	–	–	–	–	> 22.93	1
20-08-12	561 59.91	–	–	–	–	> 22.97	1
27-08-12	561 66.87	–	–	–	–	> 22.55	1
01-09-12	561 71.84	–	–	–	–	> 22.77	1
20-09-12	561 90.88	–	–	–	–	> 23.79	1
21-09-12	561 91.86	–	–	–	–	> 23.87	1
29-09-12	561 99.76	–	–	–	–	> 22.68	1
07-10-12	562 07.84	–	–	–	–	18.99 (0.06)	1
09-10-12	562 09.84	–	–	–	–	18.52 (0.06)	1
12-10-12	562 12.81	–	–	–	–	17.65 (0.02)	1
13-10-12	562 13.83	–	–	–	–	17.59 (0.03)	1
14-10-12	562 14.82	–	–	17.69 (0.03)	–	17.47 (0.02)	1
15-10-12	562 15.69	–	–	–	–	17.46 (0.02)	1
16-10-12	562 16.81	–	–	–	–	17.39 (0.02)	1
17-10-12	562 17.75	–	–	–	–	17.39 (0.02)	1
18-10-12	562 18.85	–	–	–	–	17.41 (0.02)	1
19-10-12	562 19.76	–	–	–	–	17.45 (0.02)	1

Table A1 – *continued*

Date (dd-mm-yy)	JD (+240 0000)	*U*	*B*	*V*	*R*	*I*	Instrument
20-10-12	562 20.70	–	–	–	–	17.47 (0.02)	1
20-10-12	562 20.82	–	–	–	–	17.47 (0.02)	1
21-10-12	562 21.80	–	–	17.92 (0.03)	–	17.52 (0.02)	1
25-10-12	562 25.69	–	–	–	–	17.70 (0.02)	1
26-10-12	562 26.70	–	–	–	–	17.76 (0.03)	1
28-10-12	562 28.66	–	–	–	–	17.79 (0.04)	1
29-10-12	562 29.70	–	–	–	–	17.92 (0.03)	1
30-10-12	562 30.69	–	–	–	–	17.96 (0.03)	1
31-10-12	562 31.71	–	–	–	–	18.01 (0.03)	1
31-10-12	562 31.87	–	19.31 (0.10)	18.77 (0.08)	18.50 (0.04)	18.06 (0.06)	2
01-11-12	562 32.80	–	–	–	–	18.09 (0.03)	1
02-11-12	562 33.77	–	–	–	–	18.15 (0.03)	1
04-11-12	562 35.75	–	–	–	–	18.19 (0.03)	1
06-11-12	562 37.82	–	–	–	–	18.24 (0.03)	1
07-11-12	562 38.79	–	–	–	–	18.34 (0.03)	1
08-11-12	562 39.69	–	–	–	–	18.39 (0.03)	1
08-11-12	562 39.78	–	–	–	–	18.44 (0.03)	1
10-11-12	562 41.77	–	–	–	–	18.38 (0.04)	1
11-11-12	562 42.78	–	–	–	–	18.43 (0.03)	1
12-11-12	562 43.79	–	–	–	–	18.50 (0.03)	1
14-11-12	562 45.77	–	–	20.04 (0.05)	–	18.54 (0.03)	1
17-11-12	562 48.70	–	–	–	–	18.55 (0.03)	1
20-11-12	562 51.72	–	–	–	–	18.59 (0.03)	1
22-11-12	562 53.82	–	–	20.01 (0.10)	19.53 (0.09)	–	3
22-11-12	562 53.83	–	–	20.00 (0.06)	–	–	3
23-11-12	562 54.72	–	–	–	–	18.60 (0.03)	1
26-11-12	562 57.73	–	–	–	–	18.59 (0.04)	1
01-12-12	562 62.65	–	–	–	–	18.64 (0.04)	1
04-12-12	562 65.71	–	–	–	–	18.68 (0.03)	1
06-12-12	562 67.65	–	–	20.14 (0.06)	–	–	1
08-12-12	562 69.67	–	–	20.20 (0.05)	–	18.63 (0.03)	1
09-12-12	562 70.65	–	–	–	–	18.69 (0.03)	1
12-12-12	562 73.67	–	–	20.08 (0.06)	–	18.63 (0.03)	1
13-12-12	562 74.71	–	–	–	–	18.69 (0.03)	1
19-12-12	562 80.72	–	–	–	–	18.68 (0.04)	1
23-12-12	562 84.69	–	–	–	–	18.69 (0.04)	1
26-12-12	562 87.64	–	–	–	–	18.73 (0.04)	1
31-12-12	562 92.65	–	–	–	–	18.80 (0.04)	1
04-01-13	562 96.69	–	–	–	–	18.78 (0.04)	1
08-01-13	563 00.63	–	–	–	–	18.84 (0.04)	1
14-01-13	563 06.62	–	–	–	–	18.93 (0.04)	1
20-01-13	563 12.70	19.79 (0.11)	20.58 (0.03)	20.15 (0.03)	19.84 (0.03)	19.03 (0.05)	3
22-01-13	563 14.59	–	–	–	–	19.01 (0.05)	1
24-01-13	563 16.59	–	20.59 (0.36)	20.04 (0.21)	19.80 (0.21)	19.12 (0.26)	4
26-01-13	563 18.59	–	–	19.98 (0.12)	19.78 (0.11)	–	4
27-01-13	563 19.59	–	–	20.00 (0.08)	19.76 (0.09)	–	4
29-01-13	563 21.59	–	–	–	–	19.02 (0.05)	1
29-01-13	563 21.59	–	–	20.02 (0.12)	19.79 (0.11)	–	4
31-01-13	563 23.59	–	–	20.11 (0.05)	19.66 (0.11)	–	4
31-01-13	563 23.62	–	–	–	–	18.94 (0.04)	1
31-01-13	563 23.67	19.86 (0.09)	20.55 (0.10)	20.15 (0.03)	19.83 (0.06)	19.07 (0.04)	3
31-01-13	563 23.68	19.86 (0.09)	20.58 (0.05)	–	–	–	3
01-02-13	563 24.58	–	–	–	–	19.03 (0.05)	1
02-02-13	563 25.55	–	–	20.26 (0.05)	–	19.09 (0.04)	1
02-02-13	563 25.60	–	–	20.06 (0.06)	19.70 (0.08)	19.10 (0.23)	4
03-02-13	563 26.60	–	–	19.99 (0.10)	19.73 (0.21)	–	4
04-02-13	563 27.58	–	–	20.06 (0.07)	19.60 (0.07)	19.00 (0.10)	4
05-02-13	563 28.55	–	–	20.01 (0.06)	–	19.05 (0.05)	1
05-02-13	563 28.58	–	–	20.01 (0.15)	19.75 (0.06)	19.07 (0.06)	4
09-02-13	563 32.58	–	–	20.08 (0.22)	19.59 (0.10)	19.01 (0.06)	4
11-02-13	563 34.58	–	–	–	–	19.10 (0.05)	1
11-02-13	563 34.58	–	–	20.12 (0.10)	19.87 (0.05)	19.19 (0.06)	4
14-02-13	563 37.54	–	–	20.03 (0.05)	19.75 (0.08)	–	4
16-02-13	563 39.55	–	–	–	–	19.11 (0.05)	1

Table A1 – *continued*

Date (dd-mm-yy)	JD (+240 0000)	*U*	*B*	*V*	*R*	*I*	Instrument
18-02-13	563 41.54	–	–	20.22 (0.01)	19.98 (0.08)	19.10 (0.10)	4
19-02-13	563 42.53	–	–	20.10 (0.09)	19.84 (0.01)	19.30 (0.04)	4
20-02-13	563 43.53	–	–	20.17 (0.02)	19.87 (0.13)	19.22 (0.03)	4
20-02-13	563 43.62	19.86 (0.10)	20.75 (0.11)	20.29 (0.07)	19.99 (0.06)	19.19 (0.05)	3
21-02-13	563 44.53	–	–	20.17 (0.02)	19.85 (0.05)	19.10 (0.03)	4
21-02-13	563 44.57	–	–	–	–	19.14 (0.04)	1
22-02-13	563 45.53	–	–	20.11 (0.03)	19.97 (0.05)	19.20 (0.02)	4
23-02-13	563 46.53	–	–	20.10 (0.08)	20.01 (0.35)	–	4
24-02-13	563 47.53	–	–	19.96 (0.03)	19.89 (0.13)	19.24 (0.22)	4
25-02-13	563 48.53	–	–	20.00 (0.01)	19.86 (0.08)	19.23 (0.03)	4
25-02-13	563 48.55	–	–	–	–	19.17 (0.07)	1
26-02-13	563 49.53	–	–	20.09 (0.02)	19.96 (0.02)	19.23 (0.03)	4
28-02-13	563 51.51	–	–	20.18 (0.15)	–	19.14 (0.07)	1
01-03-13	563 52.53	–	–	20.07 (0.03)	20.00 (0.03)	19.25 (0.03)	4
01-03-13	563 52.55	–	–	–	–	19.35 (0.08)	1
02-03-13	563 53.56	–	–	–	–	19.36 (0.07)	1
03-03-13	563 54.53	–	–	–	–	19.22 (0.07)	1
03-03-13	563 54.53	19.96 (0.04)	20.78 (0.04)	20.32 (0.03)	20.02 (0.03)	19.32 (0.02)	3
05-03-13	563 56.53	–	–	20.29 (0.01)	20.09 (0.01)	19.45 (0.11)	4
09-03-13	563 60.53	–	–	20.23 (0.05)	20.02 (0.01)	19.24 (0.03)	4
11-03-13	563 62.52	–	–	–	–	19.33 (0.06)	1
12-03-13	563 63.50	–	–	–	–	19.42 (0.13)	1
14-03-13	563 65.53	–	–	20.24 (0.02)	19.97 (0.05)	19.34 (0.03)	5
17-03-13	563 68.50	–	–	–	–	19.43 (0.08)	1
17-03-13	563 68.57	20.14 (0.07)	20.88 (0.09)	20.45 (0.09)	–	–	3
18-03-13	563 69.54	–	–	–	–	19.36 (0.05)	1
19-03-13	563 70.50	–	–	–	–	19.36 (0.11)	1
20-03-13	563 72.49	–	–	–	–	19.38 (0.09)	1
23-03-13	563 74.51	–	–	–	–	19.62 (0.09)	1
25-03-13	563 76.51	–	–	–	–	19.64 (0.13)	1
03-04-13	563 85.51	20.37 (0.04)	21.08 (0.05)	20.65 (0.04)	20.36 (0.04)	19.69 (0.03)	3
03-04-13	563 86.49	–	–	–	–	19.64 (0.09)	1
06-04-13	563 88.51	20.40 (0.10)	21.12 (0.09)	20.69 (0.06)	20.42 (0.04)	19.73 (0.05)	3
14-04-13	563 96.50	–	21.32 (0.10)	20.81 (0.05)	20.50 (0.05)	19.80 (0.09)	3
18-04-13	564 01.49	20.74 (0.16)	–	–	–	–	3
19-04-13	564 02.48	–	–	20.98 (0.20)	–	–	3
01-08-13	565 05.90	–	–	–	–	21.86 (0.55)	1
10-08-13	565 14.85	–	–	–	–	> 22.85	1
17-08-13	565 21.80	–	–	–	–	> 23.04	1
20-08-13	565 24.88	–	–	–	–	> 22.71	1

Notes. 1 = 1.3-m Warsaw University Telescope + OGLE-IV mosaic camera (Las Campanas Observatory); 2 = 2.2-m MPI/ESO Telescope + GROND (ESO-La Silla Observatory); 3 = 3.58-m New Technology Telescope + EFOSC2 (ESO-La Silla Observatory); 4 = LCOGT 1.0m-05 telescope + SBIG STX-16083 with Kodak KAF-16803 FI (Cerro Tololo Inter-American Observatory); 5 = LCOGT 1.0m-09 telescope + SBIG STX-16083 with Kodak KAF-16803 FI (Cerro Tololo Inter-American Observatory).

Table A2. NIR photometry of OGLE-2012-SN-006.

Date (dd-mm-yy)	JD (+240 0000)	*J*	*H*	*K*	Instrument
31-10-12	562 31.87	16.82 (0.06)	15.77 (0.06)	15.02 (0.08)	1
29-01-13	563 21.57	17.62 (0.06)	16.54 (0.05)	15.50 (0.07)	2
08-02-13	563 31.61	17.81 (0.09)	–	–	2
22-02-13	563 45.73	17.92 (0.08)	17.14 (0.18)	15.96 (0.11)	2
13-03-13	563 64.51	18.18 (0.07)	17.62 (0.10)	16.23 (0.08)	2
12-04-13	563 94.51	18.50 (0.10)	17.70 (0.11)	16.41 (0.09)	2
18-04-13	564 00.53	18.51 (0.06)	17.68 (0.07)	16.43 (0.07)	2

Notes. 1 = 2.2-m MPI/ESO Telescope + GROND (ESO-La Silla Observatory);
2 = 3.58-m New Technology Telescope + SOFI (ESO-La Silla Observatory).

Table A3. Magnitudes of the sequence stars in the field of OGLE-2012-SN-006. For the optical bands, errors in brackets are the rms of the magnitudes obtained averaging estimates obtained in photometric nights. The NIR magnitudes and the associated errors are those reported in the 2MASS catalogue (Skrutskie et al. 2006).

Star	*U*	*B*	*V*	*R*	*I*	*J*	*H*	*K*
1	20.784 (0.035)	19.282 (0.021)	17.515 (0.012)	16.195 (0.010)	14.518 (0.020)	12.919 (0.027)	12.338 (0.022)	11.983 (0.019)
2	20.446 (0.025)	20.220 (0.059)	19.417 (0.014)	18.979 (0.012)	18.523 (0.023)	–	–	–
3	18.712 (0.030)	18.848 (0.011)	18.129 (0.005)	17.709 (0.007)	17.298 (0.017)	–	–	–
4	17.637 (0.064)	17.172 (0.172)	16.289 (0.004)	15.789 (0.008)	15.358 (0.021)	14.800 (0.047)	14.313 (0.053)	14.243 (0.088)
5	–	20.322 (0.020)	18.525 (0.004)	17.324 (0.011)	15.682 (0.056)	14.262 (0.032)	13.634 (0.035)	13.390 (0.038)
6	–	20.464 (0.045)	18.827 (0.017)	17.572 (0.040)	16.112 (0.049)	14.489 (0.048)	13.830 (0.058)	13.480 (0.125)
7	18.429 (0.023)	17.127 (0.013)	15.620 (0.004)	14.699 (0.007)	13.705 (0.050)	12.650 (0.027)	11.949 (0.023)	11.762 (0.026)
8	20.746 (0.040)	19.329 (0.021)	17.779 (0.006)	16.782 (0.009)	15.630 (0.031)	14.458 (0.029)	13.791 (0.033)	13.620 (0.048)
9	21.164 (0.023)	19.936 (0.017)	18.355 (0.008)	17.281 (0.009)	15.925 (0.022)	14.668 (0.045)	14.115 (0.048)	13.729 (0.061)
10	21.419 (0.055)	19.989 (0.017)	18.411 (0.004)	17.496 (0.009)	16.534 (0.034)	15.512 (0.067)	14.916 (0.074)	14.536 (0.108)
11	21.577 (0.072)	20.554 (0.018)	18.998 (0.006)	18.089 (0.024)	17.147 (0.026)	15.997 (0.115)	15.312 (0.116)	15.075 (0.176)
12	–	21.546 (0.051)	20.086 (0.015)	19.159 (0.037)	18.239 (0.025)	–	–	–
13	–	–	21.393 (0.046)	20.286 (0.064)	19.108 (0.110)	–	–	–
14	–	21.636 (0.020)	20.241 (0.006)	19.318 (0.021)	18.530 (0.047)	–	–	–
15	–	–	21.983 (0.097)	21.084 (0.048)	20.258 (0.027)	–	–	–
16	16.899 (0.022)	16.477 (0.007)	15.621 (0.005)	15.159 (0.008)	14.723 (0.022)	14.116 (0.045)	13.744 (0.036)	13.616 (0.048)
17	18.908 (0.028)	17.739 (0.009)	16.600 (0.004)	15.926 (0.009)	15.359 (0.022)	14.588 (0.039)	14.045 (0.039)	13.823 (0.060)
18	20.246 (0.077)	20.504 (0.017)	19.852 (0.019)	19.455 (0.022)	19.070 (0.029)	–	–	–
19	–	–	21.135 (0.029)	20.587 (0.030)	20.076 (0.043)	–	–	–
20	18.925 (0.069)	18.909 (0.017)	18.493 (0.006)	18.241 (0.007)	18.022 (0.050)	–	–	–
21	17.614 (0.028)	17.417 (0.016)	16.590 (0.004)	16.135 (0.011)	15.716 (0.022)	15.172 (0.058)	14.934 (0.086)	14.414 (0.093)
22	21.755 (0.166)	20.450 (0.028)	18.882 (0.012)	17.770 (0.010)	16.352 (0.056)	15.026 (0.055)	14.295 (0.052)	14.173 (0.072)
23	15.584 (0.062)	15.128 (0.013)	14.215 (0.005)	13.745 (0.009)	13.351 (0.026)	12.770 (0.029)	12.371 (0.023)	12.278 (0.026)

[1]*INAF – Osservatorio Astronomico di Padova, Vicolo dell' Osservatorio 5, I-35122 Padova, Italy*
[2]*Warsaw University Observatory, Al. Ujazdowskie 4, PL-00-478 Warszawa, Poland*
[3]*Institute of Astronomy, University of Cambridge, Madingley Road, Cambridge CB3 0HA, UK*
[4]*Las Cumbres Observatory Global Telescope Network, Inc., Santa Barbara, CA 93117, USA*
[5]*Department of Physics, University of California Santa Barbara, Santa Barbara, CA 93106-9530, USA*
[6]*Núcleo de Astronomía de la Facultad de Ingeniería, Universidad Diego Portales, Av. Ejército 441, Santiago, Chile*
[7]*Millennium Institute of Astrophysics, Santiago, Chile*
[8]*Institut de Ciències de l'Espai (CSIC-IEEC), Campus UAB, Torre C5, 2a planta, E-08193 Barcelona, Spain*
[9]*European Southern Observatory, Alonso de Cordova 3107, Vitacura, Casilla 19001, Santiago, Chile*
[10]*Instituto de Astrofísica La Plata, IALP (CCT La Plata), CONICET-UNLP, Paseo del Bosque s/n, 1900 La Plata, Argentina*
[11]*Facultad de Ciencias Astronómicas y Geofísicas, Universidad Nacional de La Plata, Paseo del Bosque s/n, 1900 La Plata, Argentina*
[12]*Kavli Institute for the Physics and Mathematics of the Universe (WPI), The University of Tokyo, Kashiwa, Chiba 277-8583, Japan*
[13]*INAF – Osservatorio Astronomico di Capodimonte, Salita Moiariello, 16, I-80131 Napoli, Italy*
[14]*Department of Particle Physics and Astrophysics, Faculty of Physics, The Weizmann Institute of Science, Rehovot 76100, Israel*
[15]*School of Physics and Astronomy, University of Birmingham, Edgbaston, Birmingham B15 2TT, UK*
[16]*Max-Planck-Institut für extraterrestrische Physik, Giessenbachstrasse 1, D-85748 Garching, Germany*
[17]*Institut für Theoretische Physik und Astrophysik, Universität Würzburg, Emil-Fischer-Str. 31, D-97074 Würzburg, Germany*
[18]*Astrophysics Research Centre, School of Mathematics and Physics, Queen's University Belfast, Belfast BT7 1NN, UK*
[19]*6127 Wilder Lab, Department of Physics and Astronomy, Dartmouth College, Hanover, NH 03755, USA*
[20]*Instituto de Astrofísica, Pontificia Universidad Católica, Av. Vicuña Mackenna 4860, Casilla 306, Santiago 22, Chile*
[21]*Departamento de Física, Universidad de Concepción, Casilla 160-C, Concepción, Chile*
[22]*Department of Astronomy, Ohio State University, 140 West 18th Avenue, Columbus, OH 43210, USA*

This paper has been typeset from a TEX/LATEX file prepared by the author.